Available online at www.sciencedirect.com

SCIENCE DIRECT

Biochimica et Biophysica Acta 1667 (2004) 56–66

BIOCHIMICA ET BIOPHYSICA ACTA
BBA

http://www.elsevier.com/locate/bba

Components and fractions for differently bound water molecules of dipalmitoylphosphatidylcholine–water system as studied by DSC and ^{2}H-NMR spectroscopy

M. Kodama[a,*], Y. Kawasaki[a], H. Aoki[a], Y. Furukawa[b]

[a]*Department of Biochemistry, Faculty of Science, Okayama University of Science, 1-1 Ridai-cho, Okayama 700-0005, Japan*
[b]*Graduate School of Education, Hiroshima University, Higashi-Hiroshima 739-8524, Japan*

Received 7 May 2004; received in revised form 24 August 2004; accepted 31 August 2004
Available online 15 September 2004

Abstract

Differently bound water molecules of dipalmitoylphosphatidylcholine (DPPC)–H_2O system were investigated with differential scanning calorimetry (DSC). According to a method previously reported by us, the ice-melting DSC curves of the DPPC–H_2O samples of varying water contents were deconvoluted into multiple components, and the ice-melting enthalpies for the individual deconvoluted components were used to estimate average molar ice-melting enthalpies for freezable interlamellar and bulk waters, respectively. With these average molar ice-melting enthalpies, the numbers of differently bound water molecules of the DPPC–H_2O system were calculated at varying water contents and were used to construct a water distribution diagram of this system. Furthermore, to evaluate the reliability of the present DSC deconvolution method, ^{2}H-NMR T_1 measurements of DPPC–^2H_2O system were carried out at 5 °C of the gel phase temperature, and components and fractions for differently bound water (^2H_2O) molecules were estimated from the analysis of nonexponential magnetization recovery curves.

Keywords: Dipalmitoylphosphatidylcholine–water system; Differential scanning calorimetry; ^{2}H-NMR T_1 measurement; Differently bound water molecules

1. Introduction

Studies of the interaction of lipid and water molecules are the subject of many investigators and have been performed with many techniques such as X-ray diffraction [1–5], NMR spectroscopy [6–12], and differential scanning calorimetry (DSC) [13–18]. In this respect, we have developed a method to estimate the number of water molecules in the different bonding modes from the ice-melting DSC curves [15–18]. In this method, the ice-melting DSC curves of varying water contents were deconvoluted into multiple components by applying the conditions that (1) the number of deconvoluted curves is minimal, (2) the theoretical curve given by the sum of individual deconvoluted curves is best fitted to the experimental DSC curve, and (3) both the midpoint temperature and the half-height width (i.e., characterizing van't Hoff enthalpy) of each deconvoluted curve are maintained almost constant throughout all the deconvolutions for varying water contents. Although the deconvolution is performed under these limitations, the question is raised whether the number of deconvoluted components is actually comparable to the number of components for the differently bound water molecules. With a view to answering this question, in the present study, the deconvolution method was applied to dipalmitoylphosphatidylcholine (DPPC)–H_2O system, and fractions occupied by the respective deconvoluted components were calculated from individual average molar ice-melting enthalpies estimated for freezable interlamellar and bulk waters. For comparison with the DSC study, an alternative technique, ^{2}H-NMR measurements were performed for DPPC–^2H_2O system at desired water contents. In this NMR study, the spectra were

* Corresponding author. Tel.: +81 86 252 3161; fax: +81 86 255 7700.
E-mail address: kodama@dbc.ous.ac.jp (M. Kodama).

0005-2736/$ - see front matter © 2004 Elsevier B.V. All rights reserved.
doi:10.1016/j.bbamem.2004.08.015

recorded over a wide temperature range of −60 to 20 °C and the spin-lattice relaxation time (T_1) was measured at 5 °C of the gel phase temperature much more precisely than usual T_1 measurements [7,9,10].

Another purpose of this study is to investigate how the differently bound water molecules of the DPPC–water system are distributed at water contents near full hydration. Our previous DSC study for dimyristoylphosphatidylethanolamine (DMPE)–H_2O system has revealed the existence of a specific region where bulk water appears although the limiting, maximum amount of interlamellar water is not yet reached [15,18]. In this connection, the reliability of the gravimetric Luzzati method [3] has been repeatedly questioned [2,4,5,15,19–23]. Especially, Nagle et al. [22] have emphasized that it is incorrect to apply the Luzzati method to a system of multilamellar vesicles (MLV) near full hydration and there is a third kind of water (called "lake water") that fills the spaces between MLVs. Considering the concept proposed by Nagle et al., the bulk water detected in the specific region by us could be taken as the lake water rather than true bulk water in the excess water phase. From this viewpoint, the present T_1 measurement of the DPPC–^2H_2O system was performed for samples situated in the specific region.

2. Materials and methods

2.1. Materials and sample preparation

2.1.1. DPPC–H_2O samples for DSC

1,2-Dipalmitoyl-*sn*-phosphatidylcholine (DPPC) was purchased from Sigma Co., St. Louis, MO (>99%). The DPPC (approximately 30 mg) in a high-pressure crucible cell for a Mettler DSC apparatus was dehydrated under high vacuum (10^{-4} Pa) at room temperature for at least 3 days until no mass loss was detected by electroanalysis (Cahn Electrobalance). The crucible cell containing the dehydrated DPPC was sealed off in a dry box filled with dry N_2 gas and was then weighed with a microbalance. The DPPC–H_2O samples of varying water contents were prepared by successive additions of the desired amounts of water to the same dehydrated DPPC (30.5 mg in weight) with a microsyringe. Thus, only the weight of water was changed throughout the preparation of series of samples. All the samples were weighed after each addition of water and were annealed with a Mettler calorimeter by repeating thermal cycling (scanning rate of 0. 2 °C min^{-1}) at temperatures above and below the gel-to-liquid crystal phase transition until the same lipid transition peak was attained. After the annealing, the loss of water in the samples was checked with the microbalance.

2.1.2. DPPC–^2H_2O samples for NMR spectroscopy

The DPPC (approximately 200 mg) in a 5-mm NMR sample tube was dehydrated under the same conditions as those adopted for the DSC sample preparation. A value of 4.6 wt.% water, which the DPPC contains, was predetermined by the electrobalance and was used to determine the weight of dehydrated DPPC. A desired amount of ^2H_2O (99.97% D, Euriso-Top) was added to the dehydrated DPPC in the sample tube with a microsyringe in a dry box filled with dry N_2 gas and the tube was then sealed off. By reference to a water distribution diagram (Fig. 5) of the DPPC–H_2O system obtained by a DSC, three DPPC–^2H_2O samples of different water contents were prepared in the present study at ^2H_2O/DPPC molar ratios (N_w) of 7.0, 11.6, and 14.8, respectively. N_w 14.8 is the water content, at which a full hydration is reached. All the samples were annealed with a temperature-controlled water bath under the same conditions as those adopted for the DSC sample preparation. In order to ensure homogeneous mixing of these samples, ^{2}H-NMR spectra for ^2H_2O were measured at 5 °C during the periods of annealing at time intervals of 24 h, and the annealing was continued over at least several days until no change was observed in the NMR spectra.

2.2. Differential scanning calorimetry

2.2.1. DSC

DSC was performed with a Mettler TA-4000 apparatus for the DPPC–H_2O samples in the high-pressure crucible cell (pressure resistant to 10 MPa) and on heating from −70 °C to a temperature of the liquid crystal phase at a rate of 0.5 °C min^{-1}. The DSC was initiated by cooling the sample from a liquid crystal temperature directly to −70 °C.

2.2.2. Analysis of ice-melting DSC curves

A deconvolution analysis was performed with a computer program for multiple Gaussian curve analysis (ORIGIN, Microcal Software, Inc.) to separate the ice-melting DSC curves into two components, broad and sharp, for freezable interlamellar water (i.e., existing in regions between lipid bilayers) and bulk water (i.e., existing outside the bilayers), respectively, because the two components overlap at their bases. Furthermore, the component of freezable interlamellar water was deconvoluted into multiple components. The deconvolution was performed under the following conditions, i.e., both a half-height width and a midpoint temperature characteristic of each deconvoluted curve were maintained almost constant throughout all the deconvolutions for varying water contents.

2.3. ^{2}H-NMR spectroscopy

2.3.1. Temperature calibration

Temperatures monitored by a Bruker VT-2000 temperature controller using liquid N_2 were calibrated with a chemical shift, $\Delta\nu$, between the OH proton and the CH_3 protons of methanol by applying Van Geet's equation, T/K=478.6–0.286[$\Delta\nu$], scaled to 400 MHz [24].

The sample temperatures above 0 °C were maintained with an estimated accuracy ±0.2 °C over periods of

several hours studied, but for the temperatures below 0 °C, the accuracy lowered gradually with decreasing temperature, down to a value of approximately ±2 °C observed at −60 °C.

2.3.2. Measurements of ^{2}H-NMR spectra and ^{2}H-NMR spin-lattice relaxation times (T_1)

^{2}H-NMR spectra and ^{2}H-NMR spin-lattice relaxation times (T_1) for ^2H_2O in the DPPC–^2H_2O samples were measured with a Bruker ARX 400 MHz spectrometer (i.e., a high-resolution liquid NMR apparatus, because no NMR spectrometer for solids is available) using a broad band probe at a resonance frequency of 61.4 MHz. The NMR spectra were recorded at different temperatures of −60 to 20 °C with a 90° pulse. After a change in the temperature, thermal equilibrium of the samples was attained within 15 min.

The T_1 measurements were performed at 5 °C of the gel phase temperature with an inversion recovery pulse sequence, 180°–τ–90°. The 90° pulse width giving the highest signal intensity was accurately determined by changing a pulse irradiation period at short intervals of 0.1 μs and the 180° pulse width was then estimated by two times the 90° pulse width. The 90° pulse width thus obtained depended on the studied samples and ranged from 14.4 to 15.3 μs. An interpulse delay time of the pulse sequence, τ, was changed up to 1500 ms in the longest case (depending on 5 T_1). Especially, the delay times below 30 ms were changed at intervals as short as 1–2 ms. The magnetization recovery signals of varying delay times were recorded until their intensities became much less than 1% of the initial intensity observed at τ=0, and consequently in the inversion recovery data, as many as 80–130 were used for each T_1 measurement.

Additional spectrometer parameters used for data acquisition after irradiation of the 90° pulse were as follows: sweep width 100 kHz, acquisition time 1.6 s (>5 T_1) giving a dwell time 5 μs (a resolution 0.6 Hz), pre-scan delay (dead time) 45 μs. The number of recycle scans used to obtain a good S/N ratio was between 50 and 100.

2.3.3. Analysis of inversion recovery data

The magnetization recovery versus τ curves thus obtained were not a single exponential for three samples studied, indicating that the curves consist of multiple components characterized by respective T_1 values. Therefore, the recovery curves can be written as

$$\sum_i M_z(i) = \sum_i M_{z0}(i) - 2\sum_i M_{z0}(i)\exp(-t/T_1(i)) \quad (1)$$

where $M_z(i)$ and $M_{z0}(i)$ are magnetizations of component i at $t=\tau$ and t (=τ)=0, respectively. T_1 (i) is a spin-lattice relaxation time of component i. $\sum_i M_z(i)$ and $\sum_i M_{z0}(i)$ are experimentally obtained by the intensities of inversion recovery signals at $t=\tau$ and t (=τ)=0, respectively. Using the designations M_z(obs) and M_{z0}(obs) for $\sum_i M_z(i)$ and $\sum_i M_{z0}(i)$, respectively, Eq. (1) is replaced by

$$M_z(\text{obs}) = M_{z0}(\text{obs}) - 2\sum_i M_{z0}(i)\exp(-t/T_1(i)) \quad (2)$$

In the present study, the unknown parameters, $T_1(i)$ and $M_{z0}(i)$, characteristic of individual components were estimated by fitting Eq. (2) to the experimental inversion recovery data, and a fraction (composition) occupied by component i was calculated from $M_{z0}(i)/M_{z0}$(obs).

The fitting to the experimental data was performed by using a computer program (ORIGIN, Microcal Software) for multiple exponential decay curve analysis based upon a weighting nonlinear least squares procedure, and the best-fitted curve was determined with a distribution curve for a plot of weighted residual, r, against τ given by [25,26]

$$r(\tau) = (1/y(\tau))^{1/2}(y_{\text{theor}}(\tau) - y(\tau)) \quad (3)$$

where $y(\tau)$ is an experimental data and $y_{\text{theor}}(\tau)$ is a theoretical value obtained from a curve fitted to Eq. (2).

3. Results and discussion

3.1. Differential scanning calorimetry

Fig. 1 shows a series of typical DSC curves for the DPPC–H_2O samples with increasing water content expressed in the H_2O/DPPC molar ratio (N_w). The ice-melting peaks are followed by two lipid transition peaks of the gel ($L_{\beta'}$)-to-gel ($P_{\beta'}$) and subsequent gel ($P_{\beta'}$)-to-liquid crystal phase transitions (generally called the T_p and T_m transitions, respectively). Accordingly, the ice-melting behavior is derived from freezable water present in the $L_{\beta'}$ gel phase. In Fig. 2, enlarged scale ice-melting peaks are compared. The ice-melting peaks are shown to be comprised of two components, broad (a wide temperature range of −40 to about 0 °C) and sharp (a narrow temperature range around 0 °C), for the freezable interlamellar and bulk waters, respectively [14–18]. As is well known, the structure of ice is characterized by networks of hydrogen bonding formed among neighboring water molecules. So, the ice-melting temperature around 0 °C for the bulk water indicates that the structure of ice for this water is close to that of the most ordered hexagonal ice, the melting enthalpy of which is 1.436 kcal/mol H_2O [27]. While the ice-melting behavior for the freezable interlamellar water observed over a wide temperature range below 0 °C suggests that the ice for this water is present in plural structures far different from the hexagonal structure [18]. So, a deconvolution analysis was used to estimate the ice-melting enthalpies for both types of freezable water. In Fig. 3, typical results of deconvolution analysis are compared for varying water contents at N_w values of 7.0 (a), 11.6 (b), and 14.8 (c). The broad ice-melting peak for the freezable interlamellar water

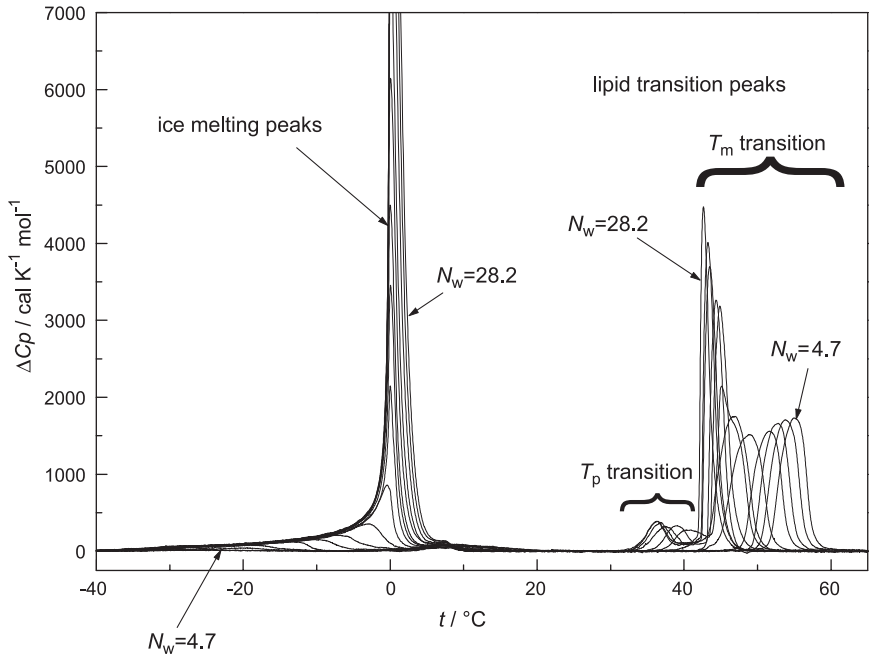

Fig. 1. A series of DSC curves of the DPPC–H_2O system ranging in H_2O/DPPC molar ratio (N_w) from 4.7 to 28.2.

was finally deconvoluted into four components, I, II, III, and IV, which successively appear with increasing water content. Therefore, the four deconvoluted components

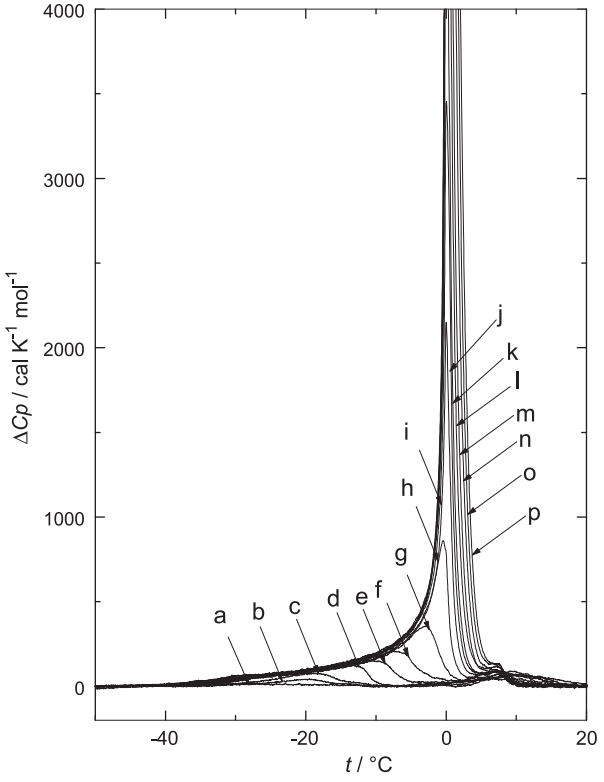

Fig. 2. A series of ice-melting DSC curves at varying H_2O/DPPC molar ratios (N_w) in the DPPC–H_2O system. N_w: (a) 4.7; (b) 5.9; (c) 6.0; (d) 6.7; (e) 7.0; (f) 7.8; (g) 8.6; (h) 10.2; (i) 11.6; (j) 12.9; (k) 14.8; (l) 16.6; (m) 19.1; (n) 21.9; (o) 24.9; (p) 28.2.

observed for the freezable interlamellar water suggest that the interlamellar water molecules form, on cooling, at least four types of ice differing in the mode of their hydrogen bonding so that the present deconvolution was performed for the minimum number of components to be best fitted to the experimental DSC curves of varying water contents. Presumably, these interlamellar water molecules are situated in positions more remote from the bilayer surfaces in the order of components I, II, III, and IV [18]. On the other hand, a single deconvoluted component V observed in Fig. 3 for N_w values of 11.6 and 14.8 is assigned to the bulk water. Additionally, in Fig. 3, a small peak is observed at approximately 5 °C higher temperatures than the ice-melting peaks. The appearance of this peak indicates a conversion of some of the gel phase into a more stable phase on cooling to −70 °C. By adequate annealing treatments, this stable phase grows up to the most stable phase, i.e., the so-called subgel phase, for which a large peak due to its transition into the gel phase is observed on heating at a high temperature of around 18 °C [23,28].

In Fig. 4a, the ice-melting enthalpies ΔH(I), ΔH(II), ΔH(III), and ΔH(IV) of the respective deconvoluted curves I, II, III, and IV for the freezable interlamellar water are plotted against N_w, together with the sum of these enthalpies, denoted as ΔH_F. In Fig. 4b, the ice-melting enthalpy ΔH(V) of the deconvoluted curve V, which gives the ice-melting enthalpy ΔH_B for the bulk water, is plotted against N_w and is compared with the ΔH_F curve for the freezable interlamellar water shown in Fig. 4a. In this figure, a ΔH_T curve is a theoretical curve obtained by assuming that all the water is present as free water. As shown in Fig. 4b, both the ΔH_F and ΔH_B (=ΔH(V)) curves gently increase in the same water content region, ~8<N_w<~15. The nonlinear increase

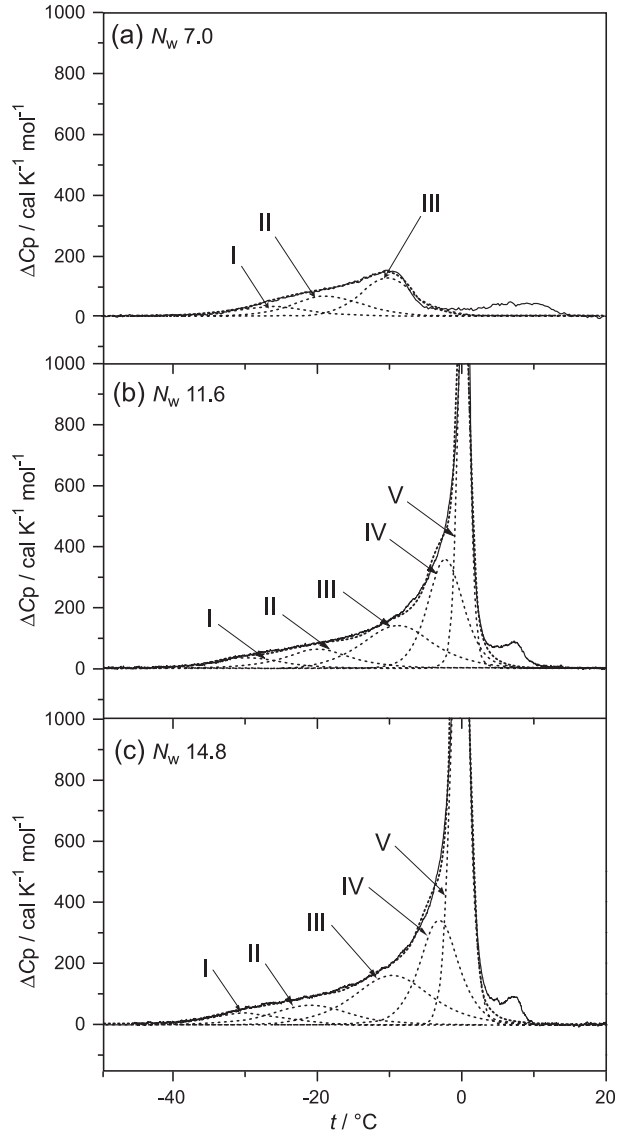

Fig. 3. Deconvolution analysis of ice-melting DSC curves at H_2O/DPPC molar ratios (N_w) of (a) 7.0, (b) 11.6, and (c) 14.8 in the DPPC–H_2O system. The deconvoluted curves I–V and their sum (the theoretical curve) are shown by dotted lines and the experimental DSC curves by solid lines.

observed for both curves is caused by the bulk water which appears, although the limiting, maximum amount of the freezable interlamellar water is not yet reached. This phenomenon indicates the existence of a specific region ($8<N_w<15$) similar to that previously reported by us for a DMPE–water system [15]. In this region, the bulk water content likewise increases, little by little, until the maximum amount of freezable interlamellar water is reached at N_w~15. Above N_w~15, all the added water is present as the bulk water, so that the ΔH_B curve becomes almost parallel to the theoretical ΔH_T line, as shown in Fig. 4b.

In Fig. 4b, the linear curves of ΔH_F ($N_w<8$) and ΔH_B ($N_w>15$) observed, except for the specific region, are characterized only by the freezable interlamellar and bulk waters, respectively, and so give individual molar melting enthalpies for both types of freezable water. On this basis, the individual average molar melting enthalpies for the freezable interlamellar and bulk water were estimated from the slopes of the respective straight ΔH_F and ΔH_B lines obtained by a least squares method. The estimated average melting enthalpies for the freezable interlamellar and bulk water are 1.187 and 1.420 kcal/mol H_2O, respectively. The average melting enthalpy for the freezable interlamellar water is fairly smaller than the known value, i.e., the melting enthalpy of the most ordered hexagonal ice (1.436 kcal/mol H_2O), obtained from the straight ΔH_T line. In this regard, the linear relationship observed between ΔH_F and N_w lower than 8 indicates that the molar ice-melting enthalpies for four deconvoluted components I, II, III and IV are not so different as expected from their different midpoint temperatures of approximately −30 to −5 °C (Fig. 3). So, the number of freezable interlamellar water molecules per molecule of lipid, denoted as N_F, was calculated from $\Delta H_F/1.187$ for varying water contents. Similarly, the number of bulk water molecules per molecule of lipid, denoted as N_B, was calculated from $\Delta H_B/1.420$. The resultant N_F and N_B values estimated for varying water contents of $N_w>5$ were summarized in Table 1, together with ΔH_F and ΔH_B values.

On the other hand, as shown in Fig. 4b, the straight ΔH_F line intersects the abscissa at N_w 5.03. Accordingly, all the water added up to N_w 5 is present as nonfreezable interlamellar water, and so the limiting, maximum number of nonfreezable interlamellar water molecules is estimated to be 5 H_2O per molecule of lipid. Presumably, the nonfreezable interlamellar water molecules exist mostly in narrow regions between adjacent lipid headgroups in an intrabilayer and form their hydrogen bondings to carbonyl ester groups of the lipid molecules. So, the interlamellar water molecules cannot form ice-like hydrogen bonds with neighboring water molecules even when cooled to extremely low temperatures [18]. Since the limiting, maximum number of nonfreezable interlamellar water molecules (i.e., 5 H_2O per molecule of lipid) is reached at N_w 5, for $N_w>5$ the total number of water molecules per molecule of lipid, denoted as N_T, is calculated from $5+N_F+N_B$. The resultant N_T values at varying water contents are added to Table 1 and are found to agree with the respective corresponding N_w values obtained from the amount of water added to the sample. This suggests that the average melting enthalpies for the freezable interlamellar (1.187 kcal/mol H_2O) and bulk water (1.420 kcal/mol H_2O) estimated according to the above-discussed method are reasonable. In Fig. 5, the cumulative numbers of nonfreezable interlamellar, freezable interlamellar and bulk water molecules per molecule of lipid given in Table 1 are plotted against N_w. The water distribution diagram indicates the following results for the gel phase of DPPC–H_2O system. The limiting, maximum numbers of nonfreezable interlamellar and freezable interlamellar water molecules is 5 H_2O and 5 (=10–5) H_2O per molecule of lipid,

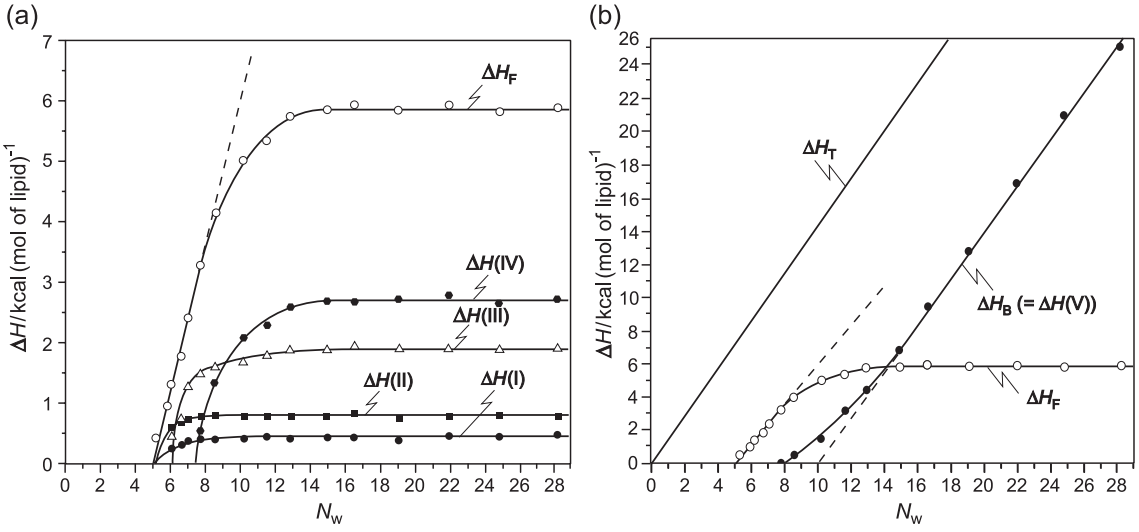

Fig. 4. (a) Plots of ice-melting enthalpies for freezable interlamellar water versus H_2O/DPPC molar ratio (N_w) in the DPPC–H_2O system. ΔH(I), ΔH(II), ΔH(III), and ΔH(IV) are the ice-melting enthalpies (per mole of DPPC) of the respective deconvoluted curves I, II, III, and IV for the freezable interlamellar water shown in Fig. 3, and ΔH_F is the sum of these individual ice-melting enthalpies. (b) A plot of the ice-melting enthalpy ΔH_B for bulk water versus H_2O/DPPC molar ratio (N_w) in the DPPC–H_2O system. ΔH_B is comparable to the ice-melting enthalpy ΔH(V) of the deconvoluted curve V shown in Fig. 3. The ΔH_F curve in panel a is shown for comparison, together with the theoretical ΔH_T curve obtained by assuming that all the water added is present as free water. Linear ΔH_F (N_w<8) and ΔH_B (N_w>15) curves obtained by a least squares method are extrapolated by dashed lines, respectively.

respectively, and are consistent with results for the gel phase of PCs obtained by other workers [23,29,30]. Furthermore, the diagram clearly shows the existence of the specific region (~8<N_w<~15) which appears before the attainment of full hydration of the gel phase.

Table 1
Ice-melting enthalpies of freezable interlamellar and bulk water, ΔH_F and ΔH_B, respectively, per mole of lipid; the numbers of freezable interlamellar and bulk water molecules, N_F and N_B, respectively, per molecule of lipid; and the total number of water molecules, N_T, per molecule of lipid at varying H_2O/DPPC molar ratios (N_w) above 5 in the DPPC–H_2O system

N_w	Ice-melting enthalphy (kcal/mol lipid)		Number of H_2O molecules per molecule of lipid		
	ΔH_F	ΔH_B	N_F	N_B	N_T[a]
5.3	0.45	0.0	0.3_8	0.0	5.3_8
6.0	0.98	0.0	0.8_3	0.0	5.8_3
6.2	1.34	0.0	1.1_3	0.0	6.1_3
6.7	1.80	0.0	1.5_2	0.0	6.5_2
7.0	2.44	0.0	2.0_6	0.0	7.0_6
7.8	3.31	0.0	2.7_9	0.0	7.7_9
8.6	4.05	0.47	3.4_1	0.3_3	8.7_4
10.2	5.03	1.41	4.2_4	0.9_9	10.2_3
11.6	5.35	3.09	4.5_1	2.1_8	11.6_9
12.9	5.75	4.43	4.8_4	3.1_2	12.9_6
14.8	5.64	7.20	4.7_5	5.0_7	14.8_2
16.6	5.95	9.42	5.0_2	6.6_3	16.6_5
19.1	5.80	12.90	4.8_9	9.0_8	18.9_7
21.9	5.96	16.99	5.0_2	11.9_6	21.9_8
24.8	5.82	21.09	4.9	14.8_4	24.7_4
28.2	5.93	25.93	5.0	18.2_6	28.2_5

ΔH_F and ΔH_B in the table generate a heat capacity function with standard deviations of 0.1–0.3 kcal K^{-1} mol^{-1}, respectively, and so an average standard deviation for N_F and N_B in the table is estimated to be 0.2.

[a] N_T is given by $5+N_F+N_B$.

3.2. ^{2}H-NMR spectroscopy

In Fig. 6, a series of typical deuteron NMR spectra at different temperatures of −60 to 20 °C is compared for two DPPC–^2H_2O samples at the ^2H_2O/DPPC molar ratios (N_w) of 7.0 (a) and 14.8 (b). For the high-resolution NMR spectrometer for liquids used in the present study, observable spectral frequency ranges are limited to several tens of kilohertz since both a 90° pulse width and a dead time

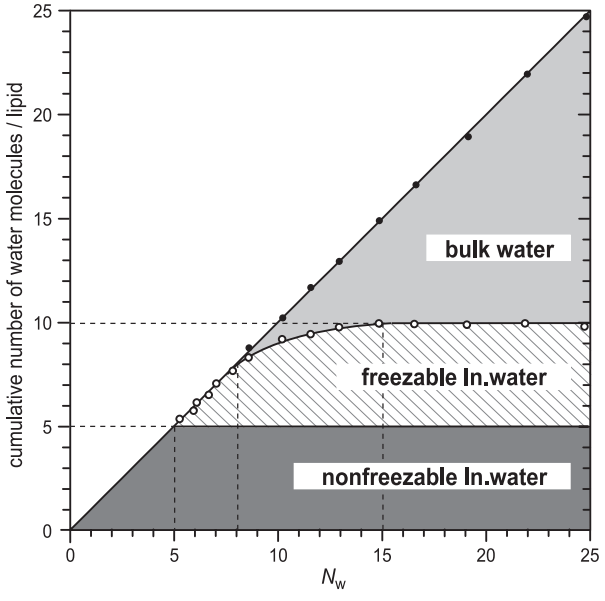

Fig. 5. Water distribution diagram for the DPPC–H_2O system. The cumulative numbers of water molecules (per molecule of DPPC) present as nonfreezable and freezable interlamellar water and as bulk water, given in Table 1, are plotted against H_2O/DPPC molar ratio (N_w).

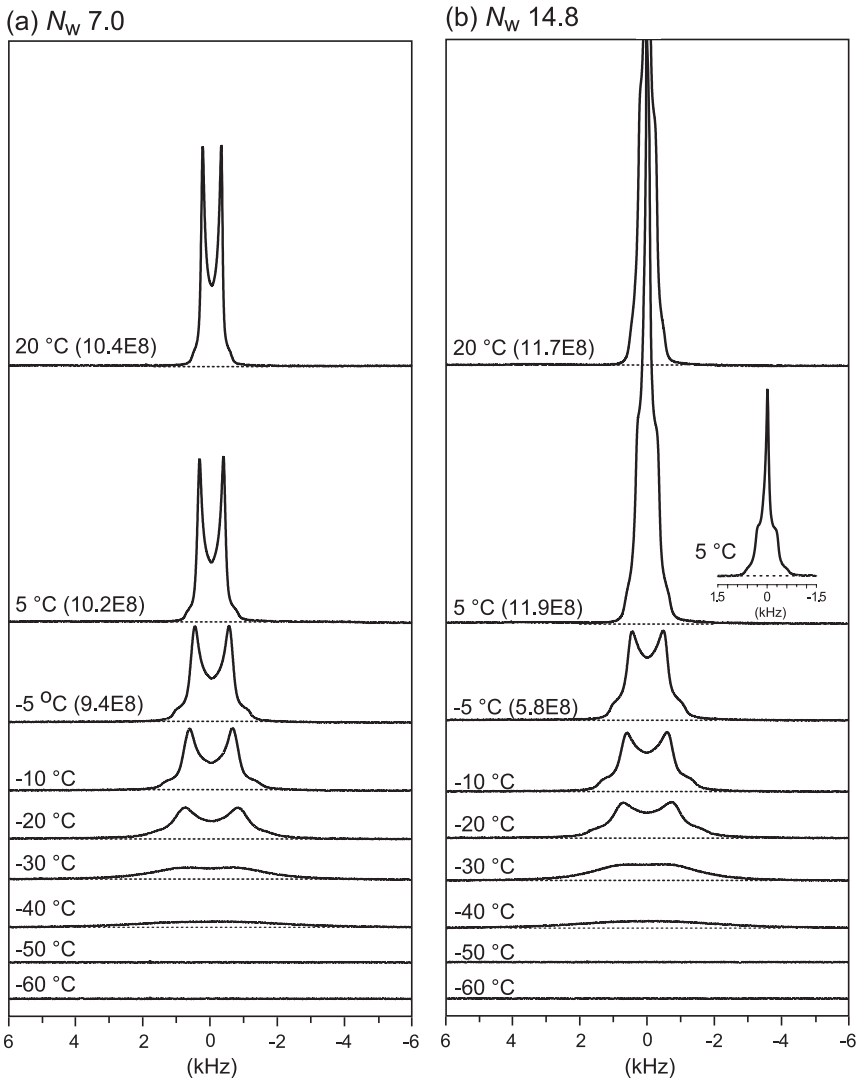

Fig. 6. Variation of ^{2}H-NMR spectra at temperatures of −60 to 20 °C for the DPPC–^2H_2O system at ^2H_2O/DPPC molar ratios (N_w) of (a) 7.0 and (b) 14.8. The temperatures, at which the NMR spectra were measured, are indicated in the figure. In panel (b) (N_w 14.8), a reduced scale NMR spectrum is also shown for a temperature of 5 °C. Values in parentheses give integrated intensities of ^{2}H spectra.

adopted are long. Accordingly, as shown in Fig. 6, no ^{2}H-NMR signals are observed at temperatures lower than −50 °C where all freezable water (^2H_2O) molecules are present in a rigid ice-like state, because the quadrupole effect of ^{2}H nucleus of these ^2H_2O molecules cause the ^{2}H signal to be spread over more than ±100 kHz. This is also the case for nonfreezable water (^2H_2O) molecules confined within the intrabilayer regions.

At first, the broad NMR spectra ranging from +4 to −4 kHz appear at a temperature around −40 °C for the two samples, indicating that a narrowing of the spectra occurs at this temperature as a result of the beginning of motions for some ^2H_2O molecules. In this connection, a point to notice in Fig. 6 is that the temperature (−40 °C), at which the spectrum shows up itself is the same as that, at which the ice obtained from the freezable interlamellar water begins to melt (Fig. 2). Such agreement in temperature suggests that the NMR spectra arise from the melted freezable interlamellar water (^2H_2O) molecules. With increasing temperature up to −5 °C, the broad spectra grow into typical quadrupole-split patterns (so-called Pake pattern). This fact indicates that the freezable interlamellar ^2H_2O molecules, even in the liquid state, undergo aspherical motions so that they are placed under the influence of DPPC headgroups present as dipolar zwitterions.

At temperatures higher than 5 °C, the behavior of spectra is far different for the two samples. As shown in Fig. 6a, for the sample at N_w 7.0 that there is no bulk water (Fig. 5), the split pattern observed at the lower temperatures is retained up to a temperature of 20 °C studied here. Furthermore, integrated intensities (given in parentheses in Fig. 6a) of the spectra observed at the higher temperatures are almost unchanged with increasing temperature and are nearly equal to that of the spectrum observed at −5 °C. These facts offer the following result that the ^{2}H signal derived from the nonfreezable ^2H_2O molecules (5 ^2H_2O/mol lipid in Fig. 5)

cannot be detected even up to 20 °C. On the other hand, as shown in Fig. 6b, for the sample at N_w 14.8 that the bulk water is present (Fig. 5), a sharp spectrum newly observed at 5 °C is shown to be superimposed on the original split one. Another noticeable point in Fig. 6b is that integrated intensities (given in parentheses) of the composite spectra are all larger by about twice than that of the split spectrum observed at −5 °C. This fact is accounted for by nearly the same number of the freezable interlamellar and bulk water molecules for the sample at N_w 14.8 (Fig. 5 and Table 1), so that the sharp spectrum is assigned to the melted bulk water present for this sample.

As discussed above, the deuteron NMR spectrum for the DPPC–^2H_2O samples can distinguish between the freezable interlamellar and bulk water. To obtain more information, measurements of ^{2}H-NMR spin-lattice relaxation time (T_1) were performed for three DPPC–^2H_2O samples of different water contents at 5 °C (the gel phase temperature) where all the freezable water is present in the liquid state. N_w values of the three samples studied were 7.0, 11.6, and 14.8, respectively.

Experimental inversion recovery data for the NMR T_1 measurements were analyzed using Eq. (2) for a system of multiple components. In Fig. 7, $[M_{z0}(\text{obs})-M_z(\text{obs})]/2M_{z0}(\text{obs})$ derived by Eq. (2) is plotted in semilogarithmic form as a function of delay time (τ). In this figure, best-fitted curves to the experimental data are shown by solid lines. All the best-fitted curves of the three samples show a nonexponential decay, indicative of multiple components characterized by different spin-lattice relaxation times. These best-fitted curves were selected on the basis of a distribution of weighted residual (r) plotted against delay time (τ) given by Eq. (3) [25,26]. For an example, in Fig. 8, the distribution of r values obtained for the sample at N_w 14.8 are compared between two (a) and three components (b). As shown in Fig. 8a, the r-distribution for the two

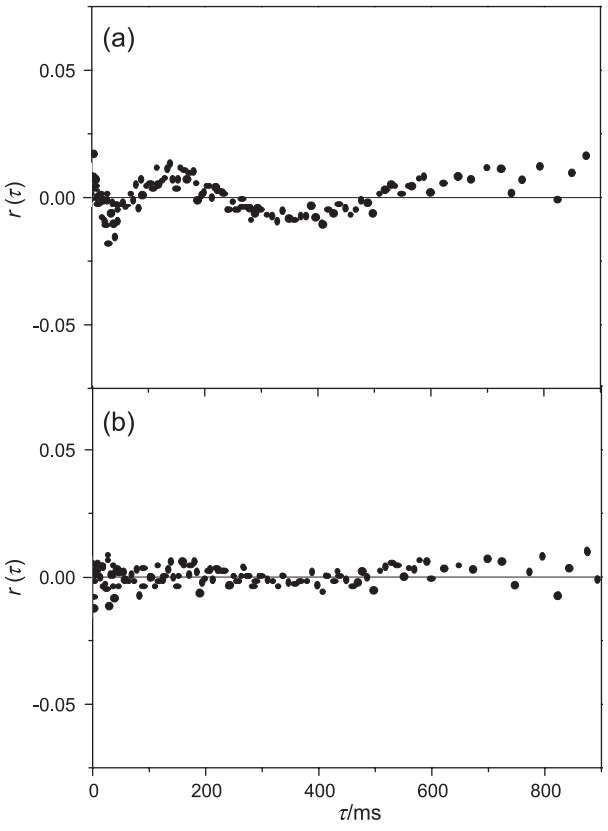

Fig. 8. A plot of weighted residual (r) versus delay time (τ) obtained for the DPPC–^2H_2O system at ^2H_2O/DPPC molar ratio (N_w) of 14.8. The weighted residual estimated for (a) two and (b) three components is compared in the figure.

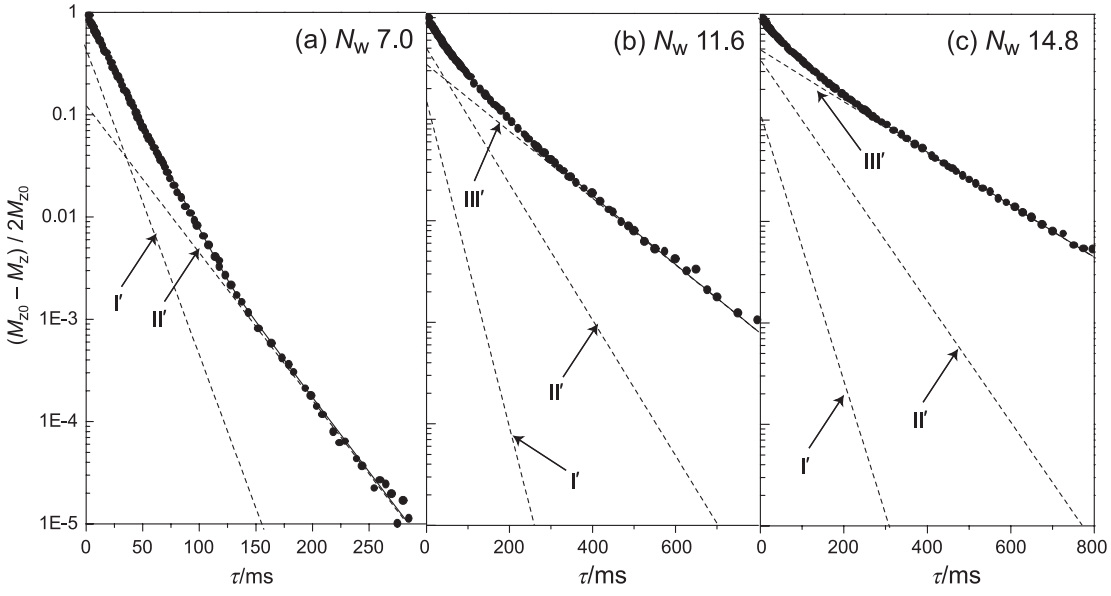

Fig. 7. Semilogarithmic plots of experimental inversion recovery data (●), $[M_{z0}(\text{obs})-M_z(\text{obs})]/2M_{z0}(\text{obs})$, versus delay time ($\tau$) for the DPPC–$^2H_2O$ system at ^2H_2O/DPPC molar ratios (N_w) of (a) 7.0, (b) 11.6, and (c) 14.8. The best-fitted curve to the experimental data is shown by a solid line. Exponential decay curves of $(M_{z0}(i)-M_z(i)/2M_{z0}(i))$ versus τ for respective components I′, II′, and III′ are shown by dashed lines.

Table 2
^{2}H spin-lattice relaxation times T_1(I′), T_1(II′), and T_1(III′) and fractions F(I′), F(II′), and F(III′) for respective components I′, II′, and III′ present as freezable water for the DPPC–^2H_2O system at ^2H_2O/DPPC molar ratios (N_w) of 7.0, 11.6, and 14.8

N_w	Component	T_1/ms		Fraction (%)	
7.0	I′	T_1(I′)	16	F(I′)	60.2
	II′	T_1(II′)	40	F(II′)	39.8
11.6	I′	T_1(I′)	27	F(I′)	15.2
	II′	T_1(II′)	55	F(II′)	50.8
	III′	T_1(III′)	140	F(III′)	34.0
14.8	I′	T_1(I′)	34	F(I′)	12.4
	II′	T_1(II′)	62	F(II′)	35.8
	III′	T_1(III′)	173	F(III′)	51.8

components is characterized by undulation, and so one component was moreover added. The resultant r-distribution for the three components is a random mode, as shown in Fig. 8b. In addition, the distribution for four components was checked to be random (data not shown), but their two components relaxed with nearly the same T_1 values. So, a fitted curve composed of the three components was selected as the best one for the sample at N_w 14.8 (Fig. 7c).

The best-fitted curve for N_w 7.0 (a) is shown to be composed of two components, denoted as I′ and II′, in contrast to three components, I′, II′, and III′, observed for N_w values 11.6 (b) and 14.8 (c). Table 2 summarizes the spin-lattice relaxation times T_1(I′), T_1(II′), and T_1(III′) of the respective components I′, II′, and III′ for the three samples. As shown in Table 2, the T_1(III′) values obtained for the two samples (N_w 11.6 and 14.8) are much longer, compared with the T_1(I′) and T_1(II′) values of these samples. Fractions F(I′), F(II′), and F(III′) of the components I′, II′, and III′ were estimated from M_{z0}(I′)/M_{z0}(obs), M_{z0}(II′)/M_{z0}(obs), and M_{z0}(III′)/M_{z0}(obs), respectively, and the results are added to Table 2.

3.3. Comparison of components and fractions between the NMR T_1 measurement and DSC

The present T_1 measurement study reveals that differently bound freezable water is present finally in three components, I′, II′, and III′, as shown in Fig. 7b (N_w 11.6) and Fig. 7c (N_w 14.8). However, the DSC deconvolution analysis for the freezable water represents five components, I, II, III, IV, and V, as shown in Fig. 3b (N_w 11.6) and Fig. 3c (N_w 14.8). Thus, there is a difference in the number of components detected by the T_1 measurement and DSC. To make clear this difference, fractions F(I), F(II), F(III), F(IV), and F(V) for the respective components I, II, III, IV, and V obtained by the DSC were estimated for the two samples at N_w values 11.6 and 14.8 and were compared with the fractions of the T_1 measurement given in Table 2. In this estimation, the numbers of water molecules (per molecule of lipid) N(I), N(II), N(III), and N(IV) for the components I, II, III, and IV present as the freezable interlamellar water were calculated from ΔH(I)/1.187, ΔH(II)/1.187, ΔH(III)/1.187, and ΔH(IV)/1.187, respectively, where $\Delta H(i)$ [i=I, II, III, and IV] is the ice-melting enthalpy per mole of lipid for component i given by Fig. 4a and 1.187 kcal/mol H_2O is the average ice-melting enthalpy for the freezable interlamellar water discussed above. Accordingly, the sum of N(I), N(II), N(III), and N(IV) gives the total number of freezable interlamellar water molecules N_F given in Table 1. While the number of water molecules N(V) (=N_B) for the component V present as the bulk water has been already given in Table 1. With these estimated numbers of water molecules, the $F(i)$ [i=I, II,. . ., V] values for five components were estimated from $N(i)$ $[i = \mathrm{I},\ \mathrm{II}..,\mathrm{V}]/\sum_{i=1}^{\mathrm{V}} N(i)(=N_F+N_B)$, respectively, and the results obtained for the two samples (N_w 11.6 and 14.8) are given in Table 3, together with values of $\Delta H(i)$ and $N(i)$ [i=I, II,. . ., V].

Table 3
Ice-melting enthalpies ΔH(I), ΔH(II), ΔH(III), ΔH(IV), and ΔH(V) per mole of lipid; the numbers of water molecules N(I), N(II), N(III), N(IV), and N(V); and fractions F(I), F(II), F(III), F(IV), and F(V) for deconvoluted ice-melting components I, II, III, IV, and V at H_2O/DPPC molar ratios (N_w) of 11.6 and 14.8 in the DPPC–H_2O system

N_w	Component	Ice-melting enthalpy (kcal/mol lipid)		Number of H_2O molecules per molecule of lipid		Fraction (%)		
11.6	I	ΔH(I)	0.45	N(I)	0.3_8	F(I)	5.6	15.7[a]
	II	ΔH(II)	0.79	N(II)	0.6_7	F(II)	10.1	
	III	ΔH(III)	1.80	N(III)	1.5_2	F(III)	22.7	51.7[b]
	IV	ΔH(IV)	2.31	N(IV)	1.9_4	F(IV)	29.0	
	V	ΔH(V) (=ΔH_B)	3.09	N(V) (=N_B)	2.1_8	F(V) (=F_B)		32.6
14.8	I	ΔH(I)	0.47	N(I)	0.4	F(I)	4.1	11.0[c]
	II	ΔH(II)	0.81	N(II)	0.6_8	F(II)	6.9	
	III	ΔH(II)	1.79	N(III)	1.5_1	F(III)	15.4	37.7[d]
	IV	ΔH(IV)	2.56	N(IV)	2.1_6	F(IV)	22.0	
	V	ΔH(V) (=ΔH_B)	7.20	N(V) (=N_B)	5.0_7	F(V) (=F_B)		51.6

Standard deviations for ΔH(I)–ΔH(V) are 0.1–0.3 kcal K^{-1} mol^{-1} and an average standard deviation for N(I)–N(V) is 0.2.
[a] A value of 15.7 is given by F(I)+F(II).
[b] A value of 51.7 is given by F(III)+F(IV).
[c] A value of 11.0 is given by F(I)+F(II).
[d] A value of 37.4 is given by F(III)+F(IV).

When the $F(i)$ values for the T_1 measurements shown in Table 2 are compared with those for the DSC shown in Table 3 at the corresponding water contents, excellent agreement is observed between the two techniques and so the following results could be obtained. Thus, the assignment of long T_1 component III′ to the bulk water is clear, because $F(\mathrm{III}')$ is recognized as nearly equal to $F(\mathrm{V})$ $(=F_B)$ for the two samples. Furthermore, on the basis of the following fact that $F(\mathrm{I}')\cong F(\mathrm{I})+F(\mathrm{II})$ and $F(\mathrm{II}')\cong F(\mathrm{III})+F(\mathrm{IV})$, two short T_1 components I′ and II′ could be assigned to the freezable interlamellar water, respectively. Presumably, ^2H_2O molecules of the shorter T_1 component I′ are less mobile and are closer to the bilayer surfaces, compared with those of the component II′. So, it is said that the present T_1 measurements made it possible to separate the freezable interlamellar water into two components although these components presumably exchange, to some extent, with each other. This is owing to the present T_1 measurements made much more precisely, compared with usual T_1 measurements for which a τ value is varied at most to 2 T_1 or to 0.1 of $(M_{z0}-M_z)/2M_{z0}$.

With regard to the multiple T_1 components discussed above, we would like to add another possible interpretation. The nonfreezable interlamellar water, for which no ^{2}H-NMR signal is observed, is presumed to exist rather separately from the freezable interlamellar water, so that the coupling, in an NMR sense, between ^{2}H-spins of the nonfreezable and freezable interlamellar water (^2H_2O) molecules is weak. Such a weak ^{2}H-spin coupling could hold also for the freezable interlamellar and bulk water (^2H_2O) molecules. This is because at the gel phase temperature of 5 °C where the present T_1 measurements were performed, it is probably impossible that the freezable interlamellar water existing inside vesicles (liposomes) in a closed form exchanges with the bulk water through the rigid, solid-like lipid bilayers. Accordingly, it may be said that the nonexponential decays observed for the magnetization recovery versus τ curves in the present study (Fig. 7) is not caused by the couplings among unlike ^{2}H-spins of the nonfreezable interlamellar, freezable interlamellar, and bulk ^2H_2O molecules [31]. So, for the present T_1 measurements, the most dominant ^{2}H-spin relaxation mechanism is adopted, which is based upon a time-fluctuation in the quadrupole interaction of ^{2}H nucleus induced by motions of the ^2H_2O molecule itself and is independent of neighboring ^{2}H-spins. On this basis, it is reasonable that the short T_1 components I′ and II′ are assigned to two types of the freezable interlamellar water and the long T_1 component III′ is to the bulk water, respectively.

Finally, we discuss the reason for which the T_1 values of component III′ for the two samples (Table 2) are fairly shorter than that (273 ms, at 5 °C) of free ^2H_2O molecules. This shows that the rate of rotational-diffusion of the bulk ^2H_2O molecules in the present study is much slower than that of the pure ^2H_2O molecules. To explain the reason for this, our attention is paid to the fact that the two samples (N_w 11.6 and 14.8) for which the bulk water is detected are situated in the specific region ranging in N_w from ~8 to ~15 (Fig. 5) discussed above. By taking up a concept proposed by Nagle et al. [22], the bulk water in the specific region is considered to exist as "lake water" (named by Nagle) which fills the space between MLVs and is distinguished from true bulk water ("ocean water") in excess water phase. Such lake-like, bulk water molecules would undergo a slow rotational-diffusion as a result of their interactions with the surface of vesicles, and hence the shortening of the $T_1(\mathrm{III}')$ values is observed for the two samples, as shown in Table 2.

Acknowledgements

This work is supported in part by Grants-in-Aid for General Scientific Research (12640568) from the Ministry of Education, Science and Culture, Japan (2001).

References

[1] M.J. Ruocco, G. Shipley, Characterization of the sub-transition of hydrated dipalmitoylphosphatidylcholine bilayers. Kinetic, hydration and structural study, Biochim. Biophys. Acta 691 (1982) 309–320.
[2] T.J. McIntosh, S. Simon, Hydration force and bilayer deformation: a reevaluation, Biochemistry 25 (1986) 4058–4066.
[3] P.R. Rand, V.A. Parsegian, Hydration forces between phospholipid bilayers, Biochim. Biophys. Acta. 988 (1989) 351–376.
[4] S. Tristram-Nagle, R. Zhang, R.M. Suter, C.R. Worthington, W.-J. Sun, J.F. Nagle, Measurement of chain tilt angle in fully hydrated bilayers of gel phase lecithins, Biophys. J. 64 (1993) 1097–1109.
[5] J.F. Nagle, R. Zhang, S. Tristram-Nagle, W. Sun, H.I. Petrache, R.M. Suter, X-ray structure determination of fully hydrated L_α phase dipalmitoylphosphatidylcholine bilayers, Biophys. J. 70 (1996) 1419–1431.
[6] J. Ulmius, H. Wennerström, G. Lindblom, G. Arvidson, Deuteron nuclear resonance studies of phase equilibria in lecithin–water system, Biochemistry 16 (1977) 5742–5745.
[7] F. Borle, J. Seelig, Hydration of *Escherichia coli* lipids, deuterium T_1 relaxation time studies of phosphatidylglycerol, phosphatidylethanolamine and phosphatidylcholine, Biochim. Biophys. Acta 735 (1983) 131–136.
[8] K. Gawrisch, W. Richter, A. Mops, P. Balgavy, K. Arnold, G. Klose, The influence of water concentration on the structure of egg yolk phospholipid/water dispersions, Stud. Biophys. 108 (1985) 5–16.
[9] F. Volke, S. Eisenblatter, J. Galle, G. Klose, Dynamic properties of water at phosphatidylcholine lipid-bilayer surfaces as seen by deuterium and pulsed field gradient proton NMR, Chem. Phys. Lipids 70 (1994) 121–131.
[10] C.-H. Hsieh, W. Wu, Structure and dynamic of primary hydration shell of phosphatidylcholine bilayers at subzero temperatures, Biophys. J. 71 (1996) 3278–3287.
[11] C. Faure, J.F. Tranchant, E. Dufourc, Determination of DMPC hydration in the L_α and $L_{\beta'}$ phases by ^{2}H solid state NMR of D_2O, FEBS Lett. 405 (1997) 263–266.
[12] H. Aoki, Y. Kawasaki, M. Kodama, Estimation of differently bound water molecules for the gel phase of dimyristoylphosphatidylethanolamine–water system as studied by DSC and ^{2}H-NMR spectroscopy, J. Biol. Phys. 28 (2002) 237–252.
[13] D. Chapman, R.M. Williams, B.D. Ladbrooke, Physical studies of phospholipids: VI. Thermotropic and lyotropic mesomorphism of some 1,2-diacyl-phosphatidylcholines (lecithins), Chem. Phys. Lipids 1 (1967) 445–475.

[14] M. Kodama, H. Inoue, Y. Tsuchida, The behavior of water molecules associated with structural changes in phosphatidylethanolamine assembly as studied by DSC, Thermochim. Acta 266 (1995) 373–384.
[15] M. Kodama, H. Aoki, H. Takahashi, I. Hatta, Interlamellar waters in dimyristoylphosphatidylethanolamine–water system as studied by calorimetry and X-ray diffraction, Biochim. Biophys. Acta 1329 (1997) 61–73.
[16] H. Aoki, M. Kodama, Calorimetric investigation of the behavior of interlamellar water in phospholipid–water systems, Thermochim. Acta 308 (1998) 77–83.
[17] M. Kodama, H. Kato, H. Aoki, The behavior of water molecules in the most stable subgel phase of dimyristoylphosphatidylethanolamine–water system as studied by differential scanning calorimetry, Thermochim. Acta 352–353 (2000) 213–221.
[18] M. Kodama, H. Aoki, Water behavior in phospholipid bilayer systems, in: N. Garti (Ed.), Surfactant Science Series, Thermal Behavior of Dispersed Systems, vol. 93, Marcel Dekker, New York, 2000, pp. 247–293.
[19] J.F. Nagle, M.C. Wiener, Structure of fully hydrated bilayer dispersions, Biochim. Biophys. Acta 942 (1988) 1–10.
[20] G. Klose, B.W. Koenig, H.W. Meyer, G. Schulze, G. Degovics, Small-angle X-ray scattering and electron microscopy of crude dispersions of swelling lipids and the influence of the morphology on the repeat distance, Chem. Phys. Lipids 47 (1988) 225–234.
[21] B.W. Koenig, H.H. Strey, K. Gawrisch, Membrane lateral compressibility determined by NMR and X-ray diffraction: effect of acyl chain polyunsaturation, Biophys. J. 73 (1997) 1957–1966.
[22] J.F. Nagle, Y. Liu, S. Tristram-Nagle, R.M. Epand, R.E. Stark, Re-analysis of magic angle spinning nuclear magnetic resonance determination of interlamellar waters in lipid bilayer dispersions, Biophys. J. 77 (1999) 2062–2065.
[23] J.F. Nagle, S. Tristram-Nagle, Structure of lipid bilayers, Biochim. Biophys. Acta 1469 (2000) 159–195.
[24] A.L. Van Geet, Calibration of the methanol and glycol nuclear magnetic resonance thermometers with a static thermistor probe, Anal. Chem. 40 (1968) 2227–2229.
[25] A.E. McKinnon, A.G. Szabo, D.R. Miller, Deconvolution of photoluminescence data, J. Phys. Chem. 81 (1977) 1564–1570.
[26] D.V. O'Connor, W.R. Ware, J.C. Andre, Deconvolution of fluorescence decay curves. A critical comparison of techniques, J. Phys. Chem. 83 (1979) 1333–1343.
[27] D. Eisenberg, W. Kauzmann, The Structure and Properties of Water, Oxford at the Clarendon Press, London, 1969, Chap. 3.
[28] M. Kodama, H. Hashigami, S. Seki, Role of water molecules in the subtransition of the L-dipalmitoylphosphatidylcholine–water system as studied by differential scanning calorimetry, J. Colloid Interface Sci. 117 (1986) 497–504.
[29] V.L. Bronshteyn, P.L. Steponkus, Calorimetric studies of freeze-induced dehydration of phospholipids, Biophys. J. 65 (1993) 1853–1865.
[30] C. Faure, L. Bonakdar, E.J. Dufourc, Determination of DMPC hydration in the L_α and $L_{\beta'}$ phases by ^2H solid state NMR of D_2O, FEBS Lett. 405 (1997) 263–266.
[31] A. Abragam, Principles of Nuclear Magnetism, Oxford University Press, 1961, Chap. 8.